Lake spray aerosol emissions alter nitrogen partitioning in the Great Lakes region

Anahita Amiri-Farahani[1], Nicole E. Olson[2], David Neubauer[3], Behrooz Roozitalab[4], Andrew P. Ault[2], Allison L. Steiner[1]

[1]Department of Climate and Space Sciences and Engineering, University of Michigan, Ann Arbor, MI 48109, USA
[2]Department of Chemistry, University of Michigan, Ann Arbor, MI 48109, USA
[3]Institute for Atmospheric and Climate Science, ETH Zrich, Zrich, Switzerland
[4]Center for Global and Regional Environmental Research, University of Iowa, Iowa City, IA, USA

Key Points:

- Parameterized wind−dependent lake spray aerosol emission fluxes based on laboratory observations
- Heterogeneous reactions of $CaCO_3$ with HNO_3 increase nitrate aerosol
- Lake spray emissions of Ca^{2+} ions alters the thermodynamic equilibrium, leading to an increase in particulate nitrate and a reduction in particulate ammonium

Corresponding author: Anahita Amiri-Farahani, farahani@umich.edu

Abstract

We develop an improved, wind-driven lake spray aerosol (LSA) emissions parameterization that resolves particle size and size-independent chemical composition, and investigate the impact of these emissions on regional chemistry in the Great Lakes region. We conduct WRF-Chem simulations for November 2015, a time period with high LSA emissions. LSA particles emitted from the surface of the Great Lakes increase particulate NO_3^- by 37% over the Great Lakes and by 13% over land, primarily due to heterogeneous reactions between $CaCO_3$ and HNO_3. Cations emitted from lake spray affect the thermodynamic equilibrium, reducing particulate NH_4^+ by 16% over the Great Lakes and by 7% over the surrounding land. This also influences gas-phase species in the region, decreasing nitric acid by up to 32% over lakes. Overall, these simulations suggest that understanding LSA and its impact on other air pollutants is important for determining health and climate effects in the Great Lakes region.

1 Introduction

Sea spray aerosol (SSA) and lake spray aerosol (LSA) are predominantly formed by the action of the wind on the surface of the ocean and fresh water, respectively. Atmospheric aerosols produced by bubble bursting are one of the greatest global sources of atmospheric particulate matter (Andreae & Rosenfeld, 2008; Lewis & Schwartz, 2004). To date, only a few ambient measurements (Slade et al., 2010; Axson et al., 2016; May et al., 2018; Olson et al., 2020) and one modeling study (Chung et al., 2011) have examined the aerosol generation of fresh water, such as the Laurentian Great Lakes. Recent studies have observed the presence of lake spray in clouds (Olson et al., 2019), and observed the size distributions and chemical composition of LSA both in the field and the laboratory (Axson et al., 2016; May et al., 2016). Here, we utilize these new measurements in a regional chemistry-meteorology model to investigate the impact of LSA emissions on regional atmospheric chemistry.

Freshwater salt concentrations are 250 times lower than saltwater and have a different composition, with $[Ca^{2+}] > [Mg^{2+}] > [Na^+] > [K^+]$ common for fresh water as compared to $[Na^+] > [Mg^{2+}] > [K^+] \sim [Ca^{2+}]$ for seawater. For freshwater, total organic carbon (TOC) concentrations are of the same order of magnitude as inorganic ion concentrations, while TOC is 10^2 to 10^4 times lower than inorganic ions in seawater (Repeta et al., 2002). LSA composition is coupled to the freshwater composition and distinct from SSA (Borduas-Dedekind et al., 2019; Axson et al., 2016), therefore it is expected that Great Lakes LSA has different heterogeneous reactivity and ability to act as cloud condensation nuclei (CCN) and ice nucleating particles (INPs) compared to SSA (Guo et al., 2018; Tang et al., 2015; Moffett, 2016; Baustian et al., 2012). LSA particles collected from Lake Michigan are composed primarily of calcium carbonate, with lower concentrations of other inorganic ions, organic species, and biological material (Axson et al., 2016). In addition to differences in chemical composition, laboratory observations of Lake Michigan freshwater shows ultrafine and accumulation modes for LSA (with mode diameters of 46 ± 6 *nm* and 180 ± 20 *nm* respectively) (May et al., 2016). Axson et al., (2016) also show that laboratory number size distributions of LSA have ultrafine and accumulation modes at 53 ± 1 and 276 ± 8 *nm*, respectively, for water samples collected from two different Great Lakes locations.

Because most of the anthropogenic aerosols in the region are acidic (Craig et al., 2018; Pye et al., 2020), the addition of new, positive cations to the region from LSA has the potential to alter the aerosol thermodynamic equilibrium. Dominantly, new cations will reduce the importance of ammonia as a neutralizing agent (Guo et al., 2018) and changes to the aerosol pH will also influence the partitioning of nitrate (Vasilakos et al., 2018; Murphy et al., 2017; Aan de Brugh et al., 2012). In addition to changes in the ther-

modynamic equilibrium, calcium carbonate can react irreversibly via heterogeneous reactions with nitric acid (HNO_3) and sulfuric acid (H_2SO_4):

$$CaCO_3(s) + 2HNO_3(g) \rightarrow Ca(NO_3)_2(s) + H_2O(g) \uparrow + CO_2(g) \uparrow \quad (1)$$

$$CaCO_3(s) + H_2SO_4(g) \rightarrow CaSO_4(s) + H_2O(g) \uparrow + CO_2(g) \uparrow \quad (2)$$

In equation 1, calcium carbonate reacts with nitric acid and produces calcium nitrate, carbon dioxide and water, thereby converting gas−phase HNO_3 into particulate NO_3^-. In equation 2, particulate SO_4^{2-} is formed. Over the lower Great Lakes region, HNO_3 concentrations are greater than H_2SO_4 by one to two orders of magnitude,therefore we expect that Equation 1 will dominate in the region. This is supported by May et al. (2018), which found that LSA transported 30 km inland over Michigan was mostly converted to $Ca(NO_3)_2$ from $CaCO_3$.

SSA and LSA are generally modeled as a function of wind speed (de Leeuw et al., 2011). Observations of wind speed and vertical aerosol profiles indicate that these particles are produced from wave−breaking when the wind speeds are high enough to produce whitecaps (greater than 4 and 3.5 ms^{-1} over ocean and the Great Lakes, respectively (Lewis & Schwartz, 2004; Slade et al., 2010). The annual mean wind speeds over the Great Lakes are greater then 6.6 ms^{-1} (except for Lake Ontario), indicating the frequent presence of wind speeds able to produce LSA (Doubrawa et al., 2015). Additionally, freshwater whitecap lifetime is shorter than saltwater (Monahan and Zietlow, 1969) and we expect that the production of LSA will be lower than those of SSA under similar meteorological conditions.

Here, we conduct WRF-Chem model simulations over the Great Lakes region in November 2015 to study the impacts of LSA particles on regional gas-phase chemistry. Simulations indicate that LSA could change the thermodynamic equilibrium that partitions gases into and out of the aerosol phase, thereby leading to increases in particulate nitrate and reductions in ammonium both over lakes and more broadly in the Great Lakes region.

2 Model description

We employ version 3.9.1 of the mesoscale Weather Research and Forecasting model with online Chemistry (WRF-Chem; Grell et al. (2005)). The physics parameterizations used in the simulations include the Morrison double−moment microphysics scheme (Morrison et al., 2009), the Rapid Radiative Transfer Model for general circulation models (RRTMG) model shortwave and longwave radiation schemes (Iacono et al., 2008), the Grell 3D ensemble (G3D) scheme for cumulus clouds (Grell & Dvnyi, 2002), and the Yonsei University (YSU) planetary boundary layer (PBL) scheme (Hong et al., 2006) coupled to the revised MM5 surface−layer scheme, and the Noah land−surface model (Chen & Dudhia, 2001).

For chemistry, we utilize the MOZART (Model for OZone And Related chemical Tracers) mechanism for gas−phase chemistry (Emmons et al., 2010), with aqueous chemistry and coupled with the MOSAIC (Model for Simulating Aerosol Interactions and Chemistry) aerosol scheme (Zaveri et al., 2008) to simulate the major aerosol components (nitrate, ammonium, sulfate, black carbon (BC), primary OM, water and other inorganic matter). MOSAIC is a sectional aerosol module that simulates particles with dry diameters between 39 nm and 10 μm, with the size range divided into either four or eight size bins. Here, we use a four bin representation with dry diameters ranging from 0.039−0.156 (Bin 1), 0.156−0.625 (Bin 2), 0.625−2.5 (Bin 3) and 2.5−10.0 (Bin 4) μm. Thermodynamic equilibrium is simulated in MOSAIC for solid−phase particles with a set of fixed

gas-particle equilibrium relationships, where calcium salts form first, followed by sodium and then ammonium salts. Therefore, the addition of Ca^{2+} ions from LSA emissions have the potential to influence the partitioning of ammonium ions. For a given cation, salts containing sulfate form first, followed by nitrate, chloride and then carbonate (Zaveri et al., 2005). These four anions are primary LSA emissions as well, therefore further influencing the salt formation. For mixed−phased and liquid−phase particles, the thermodynamic equilibrium is sensitive to changes in variables like relative humidity, pH, and particle composition. Gas−particle partitioning uses the Adaptive Step Time-Split Euler Method (ASTEM), which employs the concept of dynamic pH and separates nonvolatile and semivolatile species with different time integration methods for efficiency (Zaveri et al., 2008). Aerosols of different bin sizes can coagulate, calculated using the algorithm of (Jacobson et al., 1994) with a Brownian coagulation kernel, and transfer between bins (e.g. after gas-particle partitioning or coagulation) following the approach of Simmel and Wurzler (2006). In MOSAIC, pH is calculated as (Buck et al., 2002):

$$pH = -log_{10}(a_{H^+}) \tag{3}$$

where a_{H^+} is the activity of H^+ (mol kg^{-1}) in aqueous solution on a molality basis.

In MOSAIC the components in each individual bin are internally mixed and $CaCO_3$ is treated as solid at all relative humidity values. Observational studies suggest that the rate of heterogeneous reactions may increase with increasing RH (Preszler Prince et al. (2007)), and May et al. (2018) observed particles which had undergone heterogeneous reactions with HNO_3 to form $Ca(NO_3)_2$ in the atmosphere. In the model, $CaCO_3$ will remain solid even at relatively high relative humidity values when other aerosol components are liquid, suggesting that the model may underestimate the heterogeneous reaction rates.

The model simulations were run for one month in November 2015. In November, the surface winds reach a seasonal maximum over the lake surface, leading to the most intense lake surface emissions. The first five days were used for model spin−up and are excluded from the analysis. The model is configured with 35 vertical levels (model top at 50 hPa), 12 km horizontal resolution, covering the Great Lakes area (Figure 1c). Simulations are analyzed for a sub−domain that focuses on the Great Lakes region (outlined in Figure 1c.) Meteorological boundary conditions are from the North American Mesoscale Forecast System (NAM), with a horizontal 12 km resolution, 40 vertical levels at 6−hour intervals. Baseline anthropogenic emissions are provided by U.S. EPA NEI14 (National Emissions Inventory, base year 2014) version 2. The Model of Emissions of Gases and Aerosols from Nature (MEGAN v. 2.0.4) provides biogenic emissions (Guenther et al., 2006), with biogenic secondary organic aerosol formation from monoterpenes. Chemical initial and boundary conditions are derived from CAM-Chem (Lamarque et al., 2012).

We conduct and analyze two simulations hereinafter referred to as "NEI" and "NEI+Lake". In the NEI simulation, only the U.S. EPA NEI14 emissions are included and there are no LSA emissions from the Great Lakes. The NEI+Lake simulation considers both EPA NEI14 and Great Lakes LSA emissions. The differences between the NEI and NEI+Lake simulations represent the effects of LSA on regional chemistry.

3 LSA emissions parameterization

Chung et al. (2011) assumed that the number of droplets emitted should be similar between freshwater and marine surfaces, and the droplet number production does not depend on the lake surface water composition. However, recent work by May et al. (2016) indicated a bi-modal size distribution and lower number emission flux for LSA based on laboratory experiments (Figure 1b).

Here, we update the wind-dependent function used in Chung et al. (2011) by scaling to the laboratory observations of May et al. (2016) for Lake Michigan freshwater and synthetic seawater. The particle number flux parameterization for a marine environment (Geever et al., 2005) is:

$$log(F_{10nm}) = 0.099U_{22} - 0.73 \tag{4}$$

$$log(F_{100nm}) = 0.109U_{22} - 1.19 \tag{5}$$

where U_{22} is the horizontal wind speed at 22 m (in ms^{-1}) and F_{10nm} and F_{100nm} are the particle source fluxes (in $10^6 m^{-2} s^{-1}$) for particles with diameters larger than 10 and 100 nm. Wind speeds at 22 m are calculated using modeled surface−level wind speeds and Monin−Obukhov similarity theory with the same stability functions as those used in WRF's 10−m wind field calculations.

Since a particle number emission flux in a certain size range is proportional to the total number of emitted particles in that size range, aerosol size distributions of seawater and lakewater can be used to scale the parameterization of Geever et al. (2005). We integrate the observed aerosol number size distributions for synthetic seawater (SSA) and Lake Michigan freshwater from May et al. (2016) to be represented by the four size bins of the MOSAIC scheme:

$$log(F_{LSA,39-156nm}) = log(F_{10nm} . \frac{N_{LSA,[39-100nm]}}{N_{SSA,[>10nm]}}) + log(F_{100nm} . \frac{N_{LSA,[100-156nm]}}{N_{SSA,[>100nm]}}) \tag{6}$$

$$log(F_{LSA,156-652nm}) = log(F_{100nm} . \frac{N_{LSA,[156-652nm]}}{N_{SSA,[>100nm]}}) \tag{7}$$

where $F_{LSA,39-156nm}$ is the particle source flux of lake Michigan freshwater between 39 and 156 nm (MOSAIC Bin 1), N_{LSA}, 39−156 nm is the integrated lake Michigan freshwater size distribution between 39 and 156 nm and $N_{SSA}[> 10nm]$ and $N_{SSA}[> 100nm]$ are the integrated synthetic seawater size distribution for particles with diameters larger than 10 and 100 nm . We scale the other two bins in the model in the same way as the second bin.

The mass emission fluxes are calculated from number emission fluxes and an assumed dry particle density of 1.5 g cm^{-3} (May et al., 2018) and mean dry diameter for each bin. We calculate the mean dry diameter based on mass mean for each bin.

Emitted LSA particles are assumed to have the composition of lake surface water from Slade et al. (2010). We also add a CO_3^{2-} mass fraction to the LSA composition based on the balance between cations and anions and the 1:1 molar ratio between calcium and carbonate. Our assumptions about LSA composition broadly agree with the measurements of ambient LSA over Lake Michigan in Olson et al. (2019) and measurements of lake water compositions in Chapra et al. (2012) for all Great Lakes. The mass fractions of emitted LSA particles are 23%, 11%, 14%, 0.2%, 7%, 35%, and 9% for Ca^{2+}, Na^{+}, SO_4^{2-}, NO_3^{-}, Cl^{-}, CO_3^{2-}, and TOC, respectively (Figure 1a). In WRF-Chem, we classify measured Mg^{2+} as Na^{+}, because Mg^{2+} is not explicitly modeled in MOSAIC.

4 Results

In November 2015, simulated winds were generally southerly to southwesterly over most of the Great Lakes region (Figure 1c). Wind speeds were greater than 8 ms^{-1}, lead-

ing to LSA emissions rates on the order of $10^6 m^{-2} s^{-1}$. LSA are transported by the wind to the northeast allowing LSA to influence the atmospheric chemistry also over the land surrounding the Great Lakes. Emitted LSA particles are composed of Ca^{2+}, CO_3^{2-}, Na^+, Cl^-, SO_4^{2-}, NO_3^-, and TOC, with $CaCO_3$ accounting for 58% of the emitted mass (Figure 1a). Components that also have anthropogenic contributions (e.g., NO_3^-, SO_4^{2-}, and TOC) comprise less than 24% of the mass fraction. Because the dominant components of LSA emissions are inorganic species, and specifically include cations, they can alter the thermodynamic balance of aerosols in the region.

The amount of nitrate aerosol in the NEI+Lake simulation (Figure S1) is greater than the NEI simulation (Figure 2a-d), with the increase dominated by the larger size bins (Figures 2c and d) and slight reductions over land in the smaller size bins (Figures 2a and b). The changes in nitrate could be explained by three potential factors: (1) an increase in primary LSA emissions, (2) changes in the thermodynamic equilibrium of the particles that could promote or reduce nitrate formation, and (3) heterogeneous chemical reactions that form particulate nitrate (e.g. Equations 1 and 2). The addition of primary LSA emissions has only a minor contribution to the increase in particulate nitrate, because primary nitrate emissions comprise only 0.2% of the total emitted LSA mass. For the thermodynamic changes, the primary LSA emissions of Ca^{2+} can neutralize anions over NH_4^+ (Zaveri et al., 2005), increasing aerosol pH (Figure 2i-l) and the nitrate partitioning from the gas to the particle phase (Vasilakos et al., 2018; Aan de Brugh et al., 2012). We conducted an additional sensitivity simulation that turns off the heterogeneous calcium reactions (Equations 1 and 2) to examine the role of these reactions on the nitrate change (Figures S5 and S6). The simulations suggest that about 47% of this increase in nitrate aerosol for the two larger size bins (Figure 2c and d) over the lake regions is due to the heterogeneous reaction of $CaCO_3$ with HNO_3 (equation 1). Since anthropogenically driven reactions are included in all simulations, no substantial changes in nitrate due to anthropogenic emissions in the sensitivity simulation are expected. Gas-phase HNO_3 decreases accompany the increases in over-lake nitrate aerosol in NEI+Lake compared to NEI (Figure 3b), illustrating the transition of nitrogen from the gas to the particle phase due to both heterogeneous reactions and thermodynamic changes.

For the two smaller size bins where most of the anthropogenically-derived aerosol is present, thermodynamic changes increase nitrate over lakes, yet nitrate aerosol decreases over land (Figure 2a and b) and over the southern portion of Lake Michigan where the regional anthropogenically-driven NOx concentrations are higher (Figure 2b).

The aerosol pH for the smaller size bins ranges from about 2.5−4 over land in the NEI simulation, and pH increases slightly (0.5 pH units) over land when LSA is added (Figure 2i and j). This increase in pH does not increase the partitioning to nitrate, and suggests that the aerosol may already be sufficiently less acidic than other regions in the US where an increase in pH would enable more nitrate partitioning (e.g., Vasilakos et al. (2018)). This slight decrease in nitrate over land may be due to changes in thermodynamic equilibrium related to the overall ion balance, where additional sulfate from LSA emissions increases in the region and replaces nitrate in the smaller bins. Overall, total particulate mass is reduced slightly in the smallest two size bins over land in the NEI+Lake simulation (Figure 4b), which supports the nitrate reductions over land.

Substantial changes in particulate NH_4^+ are observed in bins 2 and 3 (Figure 2 f−g). For the conditions of the Great Lakes region, the thermodynamic model preferentially forms Ca^{2+} and Na^+ over NH_4^+ salts (Zaveri et al., 2005) and LSA provides a new source of cations to the atmosphere dominantly via Ca^{2+} emissions (and to a lesser extent, Na^+), reducing partitioning of NH_3 from the gas to the particle phase. Generally, NH_4^+ decreases over the Great Lakes in all bins except for Lake Michigan and some regions of Lakes Superior and Huron in the first bin. Because the highest ammonium concentrations are in bin 2 both over lakes and surrounding land (Figure 4a and b), ammonium concentra-

tions are reduced on average 16% over the lakes, but decreases are observed in the fine mode broadly across the entire region. As a result of the reduced formation of particulate NH_4^+, NH_3 concentrations increase in the NEI+Lake simulations over the entire domain, but particularly over water (Figure 3a).

We also investigate the southern lake Michigan and neighboring land area aerosol ion compositions to better understand the NO_3^- and NH_4^+ differences in the two simulations (Figure 4a and b; regions denoted in Figure 1c). Ion fractions and compositions are similar in the first bin over both lake and land, and the amount of LSA ions (in particular Ca^{2+}, CO_3^{2-}, Na^+, and Cl^-) is negligible, thus the difference between the two simulations for NO_3^- and NH_4^+ is small over the lakes (Figure 2a and e). In the second bin, primary LSA emissions add new cations (e.g., Ca^{2+} and Na^+,) over the lake region, leading to an increase in the overall aerosol mass (9%). Because the addition of cations alters the thermodynamic equilibrium, NH_4^+ ion fractions decrease over southern lake Michigan in NEI+Lake as compared to the NEI simulation, which is similar to the broad regional changes observed (Figure 2f). In bins 3 and 4 (the larger size bins), NO_3^- increases due to primary emissions, the heterogeneous reactions that form particulate NO_3^-, and an increase in aerosol pH which favors nitrate in the aerosol phase. In contrast, the NH_4^+ fraction for both bin 3 and 4 in the NEI+Lake simulation decreases compared to the NEI, suggesting that the LSA cations reduce the ability of NH_3 to partition to the aerosol phase. The analysis of the ion fractions in the aerosol close to the surface of Lake Michigan and the surrounding land shows that indeed the positive NH_4^+ ions are replaced by positive Ca^{2+} and Na^+ ions in NEI+Lake compared to NEI (in particular in the larger bins). Furthermore the increase in positive ions (Ca^{2+} and Na^+) leads also to an increase in NO_3^- and SO_4^{2-} anions (Figure S2). The overall aerosol mass concentrations of all aerosol species are compared to several IMPROVE sites in the model domain (Figure S3 b−f; Table S1). NEI+Lake improves agreement with the aerosol IMPROVE composition as compared to NEI, with reductions in model bias for SO_4^{2-}, NO_3^- and TOC. Comparisons with Ca^{2+}, Na^+ and Cl^- (comprising a small component of the total aerosol mass) are variable, suggesting that further data that resolves the aerosol size and composition may improve our simulations. Overall, however, the evaluation suggests that the addition of LSA provides a slight improvement of the simulated regional aerosol composition.

Additional LSA and concomitant aerosol thermodynamics alter the regional gas−phase concentrations of nitrogen species as well. Ammonia concentrations increase across the domain up to 80 ppt over lake regions (Figure 3a and S4a). HNO_3 is consumed in the heterogeneous reaction with $CaCO_3$ (equation 1) when there are LSA emissions and the amount of HNO_3 decreases compared to the simulation without lake emissions (Figure 3b and S4b). Changes in NOx are more heterogeneous than NH_3 or HNO_3, with small increases of up to 100 ppt near urban regions as nitrate partitioning decreases over the land area in the smaller size bins (Figures 2a and b).

5 Conclusions

We conduct simulations with WRF-Chem to investigate the impacts of LSA emissions on regional aerosol changes over the Great Lakes region.

In addition to the primary emissions of LSA that are dominated by calcium carbonate, simulated nitrate aerosol increases, predominantly due to irreversible heterogeneous reactions between $CaCO_3$ and HNO_3. Changes to thermodynamic equilibrium from additional LSA cations decreases smaller particulate nitrate over land, yet increases larger particulate nitrate over the entire region, leading to an overall decrease in HNO_3 when LSA emissions are included in simulations. Particulate NH_4^+ generally decreases across the Great Lakes because Ca^{2+} and Na^+ from LSA emissions provide additional competitive cations that reduce NH_3 partitioning to the particle phase in the Great Lakes area. In some regions over land where larger nitrate aerosol increases are simulated, NH_4^+

increases slightly but overall the particulate ammonium decreases and gas-phase NH_3 increases over lakes by 12% and 2% over land. The addition of LSA increases particulate matter less than 2.5 ($PM_{2.5}$) and 10 microns in diameter (PM_{10}) by 0.78 (24%) and 1.01 (24%) $\mu g\ m^{-3}$ over lakes, with an increase of $PM_{2.5}$ and PM_{10} by 0.16 (5%) and 0.2 (4%) $\mu g\ m^{-3}$ over the surrounding land. Particulate matter greater than 2.5 microns and less than 10 microns increases by 0.23 (25%) $\mu g\ m^{-3}$ over lakes and 0.04 (3%) $\mu g\ m^{-3}$ over the surrounding land. Nitrate can represent a large fraction of aerosol in some urban and agricultural regions and is expected to become likely more important SO_2 and NOx decreases and NH_3 increases(Bian et al., 2017). Because LSA emissions affect the H_2SO_4, HNO_3 and NH_3 concentrations, it is necessary to account for LSA emissions when studying the trend of future aerosol composition, specifically nitrate, in the Great Lakes region.

The effects of LSA emissions on aerosol−cloud interactions is unknown. Olson et al. (2019) show that LSA can act as CCN and possibly INPs over the Great Lakes, which could potentially influence lake−effect cloud formation and properties. This could change cloud microphysical and radiative properties in the Great Lakes region, and other areas with large bodies of freshwater. Further modeling work is needed to investigate the aerosol−cloud interactions in the Great Lakes area. Furthermore, for a more realistic representation of LSA in model simulations measurements of the size−resolved aerosol composition are needed. Additionally, LSA can contain large amounts of organics in the presence of harmful algal blooms, which can be harmful to human health (May et al., 2016, 2018), which are not included in these simulations. Based on the work presented here, future work can explore the role of LSA emissions on coupled cloud chemistry and human health impacts.

Acknowledgments

Funding for this project was provided by the University of Michigan Cooperative Institute for Great Lakes Research (CIGLR), through the National Oceanic and Atmospheric Administration (NOAA) Cooperative Agreement NA17OAR4320152.

The data model simulations analyzed during the current study are available on: https://doi.org/10.7302/y2q
7f47.

References

Aan de Brugh, J. M. J., Henzing, J. S., Schaap, M., Morgan, W. T., van Heerwaarden, C. C., Weijers, E. P., ... Krol, M. C. (2012). Modelling the partitioning of ammonium nitrate in the convective boundary layer. *Atmospheric Chemistry and Physics*, *12*(6), 3005–3023. Retrieved from `https://acp.copernicus.org/articles/12/3005/2012/` doi: 10.5194/acp-12-3005-2012

Andreae, M., & Rosenfeld, D. (2008). Aerosolcloudprecipitation interactions. part 1. the nature and sources of cloud-active aerosols. *Earth-Science Reviews*, *89*(1), 13 - 41. Retrieved from `http://www.sciencedirect.com/science/article/pii/S0012825208000317` doi: https://doi.org/10.1016/j.earscirev.2008.03.001

Axson, J. L., May, N. W., Coln-Bernal, I. D., Pratt, K. A., & Ault, A. P. (2016). Lake spray aerosol: A chemical signature from individual ambient particles. *Environmental Science & Technology*, *50*(18), 9835-9845. Retrieved from `https://doi.org/10.1021/acs.est.6b01661` (PMID: 27548099) doi: 10.1021/acs.est.6b01661

Baustian, K. J., Cziczo, D. J., Wise, M. E., Pratt, K. A., Kulkarni, G., Hallar, A. G., & Tolbert, M. A. (2012). Importance of aerosol composition, mixing

state, and morphology for heterogeneous ice nucleation: A combined field and laboratory approach. *Journal of Geophysical Research: Atmospheres*, *117*(D6). Retrieved from https://agupubs.onlinelibrary.wiley.com/doi/abs/10.1029/2011JD016784 doi: 10.1029/2011JD016784

Bian, H., Chin, M., Hauglustaine, D. A., Schulz, M., Myhre, G., Bauer, S. E., ... Tsyro, S. G. (2017). Investigation of global particulate nitrate from the aerocom phase iii experiment. *Atmospheric Chemistry and Physics*, *17*(21), 12911–12940. Retrieved from https://acp.copernicus.org/articles/17/12911/2017/ doi: 10.5194/acp-17-12911-2017

Borduas-Dedekind, N., Ossola, R., David, R. O., Boynton, L. S., Weichlinger, V., Kanji, Z. A., & McNeill, K. (2019). Photomineralization mechanism changes the ability of dissolved organic matter to activate cloud droplets and to nucleate ice crystals. *Atmospheric Chemistry and Physics*, *19*(19), 12397–12412. Retrieved from https://acp.copernicus.org/articles/19/12397/2019/ doi: 10.5194/acp-19-12397-2019

Buck, R. P., Rondinini, S., Covington, A. K., Baucke, F. G. K., Brett, C. M. A., Camoes, M. F., ... Wilson, G. S. (2002). Measurement of ph. definition, standards, and procedures (iupac recommendations 2002). *Pure and Applied Chemistry*, *74*(11), 2169–2200. Retrieved from https://doi.org/10.1351/pac200274112169 doi: doi:10.1351/pac200274112169

Chapra, S. C., Dove, A., & Warren, G. J. (2012). Long-term trends of great lakes major ion chemistry. *Journal of Great Lakes Research*, *38*(3), 550-560. Retrieved from https://www.sciencedirect.com/science/article/pii/S0380133012001384 doi: https://doi.org/10.1016/j.jglr.2012.06.010

Chen, F., & Dudhia, J. (2001, 04). Coupling an Advanced Land SurfaceHydrology Model with the Penn StateNCAR MM5 Modeling System. Part I: Model Implementation and Sensitivity. *Monthly Weather Review*, *129*(4), 569-585. Retrieved from https://doi.org/10.1175/1520-0493(2001)129<0569:CAALSH>2.0.CO;2 doi: 10.1175/1520-0493(2001)129⟨0569:CAALSH⟩2.0.CO;2

Chung, S. H., Basarab, B. M., & VanReken, T. M. (2011). Regional impacts of ultrafine particle emissions from the surface of the great lakes. *Atmospheric Chemistry and Physics*, *11*(24), 12601–12615. Retrieved from https://acp.copernicus.org/articles/11/12601/2011/ doi: 10.5194/acp-11-12601-2011

Craig, R. L., Peterson, P. K., Nandy, L., Lei, Z., Hossain, M. A., Camarena, S., ... Ault, A. P. (2018). Direct determination of aerosol ph: Size-resolved measurements of submicrometer and supermicrometer aqueous particles. *Analytical Chemistry*, *90*(19), 11232-11239. Retrieved from https://doi.org/10.1021/acs.analchem.8b00586 (PMID: 30203960) doi: 10.1021/acs.analchem.8b00586

de Leeuw, G., Andreas, E. L., Anguelova, M. D., Fairall, C. W., Lewis, E. R., O'Dowd, C., ... Schwartz, S. E. (2011). Production flux of sea spray aerosol. *Reviews of Geophysics*, *49*(2). Retrieved from https://agupubs.onlinelibrary.wiley.com/doi/abs/10.1029/2010RG000349 doi: 10.1029/2010RG000349

Doubrawa, P., Barthelmie, R. J., Pryor, S. C., Hasager, C. B., Badger, M., & Karagali, I. (2015). Satellite winds as a tool for offshore wind resource assessment: The great lakes wind atlas. *Remote Sensing of Environment*, *168*, 349 - 359. Retrieved from http://www.sciencedirect.com/science/article/pii/S0034425715300651 doi: https://doi.org/10.1016/j.rse.2015.07.008

Emmons, L. K., Walters, S., Hess, P. G., Lamarque, J.-F., Pfister, G. G., Fillmore, D., ... Kloster, S. (2010). Description and evaluation of the model for ozone and related chemical tracers, version 4 (mozart-4). *Geoscientific Model Development*, *3*(1), 43–67. Retrieved from https://gmd.copernicus.org/articles/3/43/2010/ doi: 10.5194/gmd-3-43-2010

Geever, M., O'Dowd, C. D., van Ekeren, S., Flanagan, R., Nilsson, E. D., de Leeuw, G., & Rannik, . (2005). Submicron sea spray fluxes. *Geophysical Research Letters*, *32*(15). Retrieved from https://agupubs.onlinelibrary.wiley.com/doi/abs/10.1029/2005GL023081 doi: 10.1029/2005GL023081

Grell, G. A., & Dvnyi, D. (2002). A generalized approach to parameterizing convection combining ensemble and data assimilation techniques. *Geophysical Research Letters*, *29*(14), 38-1-38-4. Retrieved from https://agupubs.onlinelibrary.wiley.com/doi/abs/10.1029/2002GL015311 doi: 10.1029/2002GL015311

Grell, G. A., Peckham, S. E., Schmitz, R., McKeen, S. A., Frost, G., Skamarock, W. C., & Eder, B. (2005). Fully coupled online chemistry within the wrf model. *Atmospheric Environment*, *39*(37), 6957 - 6975. Retrieved from http://www.sciencedirect.com/science/article/pii/S1352231005003560 doi: https://doi.org/10.1016/j.atmosenv.2005.04.027

Guenther, A., Karl, T., Harley, P., Wiedinmyer, C., Palmer, P. I., & Geron, C. (2006). Estimates of global terrestrial isoprene emissions using megan (model of emissions of gases and aerosols from nature). *Atmospheric Chemistry and Physics*, *6*(11), 3181–3210. Retrieved from https://acp.copernicus.org/articles/6/3181/2006/ doi: 10.5194/acp-6-3181-2006

Guo, H., Nenes, A., & Weber, R. J. (2018). The underappreciated role of nonvolatile cations in aerosol ammonium-sulfate molar ratios. *Atmospheric Chemistry and Physics*, *18*(23), 17307–17323. Retrieved from https://acp.copernicus.org/articles/18/17307/2018/ doi: 10.5194/acp-18-17307-2018

Hong, S.-Y., Noh, Y., & Dudhia, J. (2006, 09). A New Vertical Diffusion Package with an Explicit Treatment of Entrainment Processes. *Monthly Weather Review*, *134*(9), 2318-2341. Retrieved from https://doi.org/10.1175/MWR3199.1 doi: 10.1175/MWR3199.1

Iacono, M. J., Delamere, J. S., Mlawer, E. J., Shephard, M. W., Clough, S. A., & Collins, W. D. (2008). Radiative forcing by long-lived greenhouse gases: Calculations with the aer radiative transfer models. *Journal of Geophysical Research: Atmospheres*, *113*(D13). Retrieved from https://agupubs.onlinelibrary.wiley.com/doi/abs/10.1029/2008JD009944 doi: 10.1029/2008JD009944

Jacobson, M. Z., Turco, R. P., Jensen, E. J., & Toon, O. B. (1994). Modeling coagulation among particles of different composition and size. *Atmospheric Environment*, *28*(7), 1327-1338. Retrieved from https://www.sciencedirect.com/science/article/pii/1352231094902801 doi: https://doi.org/10.1016/1352-2310(94)90280-1

Lamarque, J.-F., Emmons, L. K., Hess, P. G., Kinnison, D. E., Tilmes, S., Vitt, F., ... Tyndall, G. K. (2012). Cam-chem: description and evaluation of interactive atmospheric chemistry in the community earth system model. *Geoscientific Model Development*, *5*(2), 369–411. Retrieved from https://gmd.copernicus.org/articles/5/369/2012/ doi: 10.5194/gmd-5-369-2012

Lewis, E. R., & Schwartz, S. E. (2004, January). Sea Salt Aerosol Production: Mechanisms, Methods, Measurements and Models—A Critical Review. *Washington DC American Geophysical Union Geophysical Monograph Series*, *152*, 3719. doi: 10.1029/GM152

May, N. W., Axson, J. L., Watson, A., Pratt, K. A., & Ault, A. P. (2016). Lake spray aerosol generation: a method for producing representative particles from freshwater wave breaking. *Atmospheric Measurement Techniques*, *9*(9), 4311–4325. Retrieved from https://amt.copernicus.org/articles/9/4311/2016/ doi: 10.5194/amt-9-4311-2016

May, N. W., Gunsch, M. J., Olson, N. E., Bondy, A. L., Kirpes, R. M., Bertman, S. B., ... Pratt, K. A. (2018). Unexpected contributions of sea spray and lake spray aerosol to inland particulate matter. *Environmental Science & Tech-*

nology Letters, *5*(7), 405-412. Retrieved from https://doi.org/10.1021/acs.estlett.8b00254 doi: 10.1021/acs.estlett.8b00254

Moffett, B. F. (2016, 05). Fresh water ice nuclei. *Fundamental and Applied Limnology*, *188*(1), 19-23. Retrieved from http://dx.doi.org/10.1127/fal/2016/0851 doi: 10.1127/fal/2016/0851

Morrison, H., Thompson, G., & Tatarskii, V. (2009, 03). Impact of Cloud Microphysics on the Development of Trailing Stratiform Precipitation in a Simulated Squall Line: Comparison of One- and Two-Moment Schemes. *Monthly Weather Review*, *137*(3), 991-1007. Retrieved from https://doi.org/10.1175/2008MWR2556.1 doi: 10.1175/2008MWR2556.1

Murphy, J. G., Gregoire, P. K., Tevlin, A. G., Wentworth, G. R., Ellis, R. A., Markovic, M. Z., & VandenBoer, T. C. (2017). Observational constraints on particle acidity using measurements and modelling of particles and gases. *Faraday Discuss.*, *200*, 379-395. Retrieved from http://dx.doi.org/10.1039/C7FD00086C doi: 10.1039/C7FD00086C

Olson, N. E., Cooke, M. E., Shi, J. H., Birbeck, J. A., Westrick, J. A., & Ault, A. P. (2020). Harmful algal bloom toxins in aerosol generated from inland lake water. *Environmental Science & Technology*, *54*(8), 4769-4780. Retrieved from https://doi.org/10.1021/acs.est.9b07727 (PMID: 32186187) doi: 10.1021/acs.est.9b07727

Olson, N. E., May, N. W., Kirpes, R. M., Watson, A. E., Hajny, K. D., Slade, J. H., ... Ault, A. P. (2019). Lake spray aerosol incorporated into great lakes clouds. *ACS Earth and Space Chemistry*, *3*(12), 2765-2774. Retrieved from https://doi.org/10.1021/acsearthspacechem.9b00258 doi: 10.1021/acsearthspacechem.9b00258

Preszler Prince, A., Grassian, V. H., Kleiber, P., & Young, M. A. (2007). Heterogeneous conversion of calcite aerosol by nitric acid. *Phys. Chem. Chem. Phys.*, *9*, 622-634. Retrieved from http://dx.doi.org/10.1039/B613913B doi: 10.1039/B613913B

Pye, H. O. T., Nenes, A., Alexander, B., Ault, A. P., Barth, M. C., Clegg, S. L., ... Zuend, A. (2020). The acidity of atmospheric particles and clouds. *Atmospheric Chemistry and Physics*, *20*(8), 4809–4888. Retrieved from https://acp.copernicus.org/articles/20/4809/2020/ doi: 10.5194/acp-20-4809-2020

Repeta, D. J., Quan, T. M., Aluwihare, L. I., & Accardi, A. (2002). Chemical characterization of high molecular weight dissolved organic matter in fresh and marine waters. *Geochimica et Cosmochimica Acta*, *66*(6), 955 - 962. Retrieved from http://www.sciencedirect.com/science/article/pii/S0016703701008304 doi: https://doi.org/10.1016/S0016-7037(01)00830-4

Simmel, M., & Wurzler, S. (2006). Condensation and activation in sectional cloud microphysical models. *Atmospheric Research*, *80*(2), 218-236. Retrieved from https://www.sciencedirect.com/science/article/pii/S0169809505002115 doi: https://doi.org/10.1016/j.atmosres.2005.08.002

Slade, J. H., VanReken, T. M., Mwaniki, G. R., Bertman, S., Stirm, B., & Shepson, P. B. (2010). Aerosol production from the surface of the great lakes. *Geophysical Research Letters*, *37*(18). Retrieved from https://agupubs.onlinelibrary.wiley.com/doi/abs/10.1029/2010GL043852 doi: 10.1029/2010GL043852

Tang, M. J., Whitehead, J., Davidson, N. M., Pope, F. D., Alfarra, M. R., McFiggans, G., & Kalberer, M. (2015). Cloud condensation nucleation activities of calcium carbonate and its atmospheric ageing products. *Phys. Chem. Chem. Phys.*, *17*, 32194-32203. Retrieved from http://dx.doi.org/10.1039/C5CP03795F doi: 10.1039/C5CP03795F

Vasilakos, P., Russell, A., Weber, R., & Nenes, A. (2018). Understanding nitrate formation in a world with less sulfate. *Atmospheric Chemistry and*

Physics, *18*(17), 12765–12775. Retrieved from https://acp.copernicus.org/articles/18/12765/2018/ doi: 10.5194/acp-18-12765-2018

Zaveri, R. A., Easter, R. C., Fast, J. D., & Peters, L. K. (2008). Model for simulating aerosol interactions and chemistry (mosaic). *Journal of Geophysical Research: Atmospheres*, *113*(D13). Retrieved from https://agupubs.onlinelibrary.wiley.com/doi/abs/10.1029/2007JD008782 doi: 10.1029/2007JD008782

Zaveri, R. A., Easter, R. C., & Peters, L. K. (2005). A computationally efficient multicomponent equilibrium solver for aerosols (mesa). *Journal of Geophysical Research: Atmospheres*, *110*(D24). Retrieved from https://agupubs.onlinelibrary.wiley.com/doi/abs/10.1029/2004JD005618 doi: 10.1029/2004JD005618

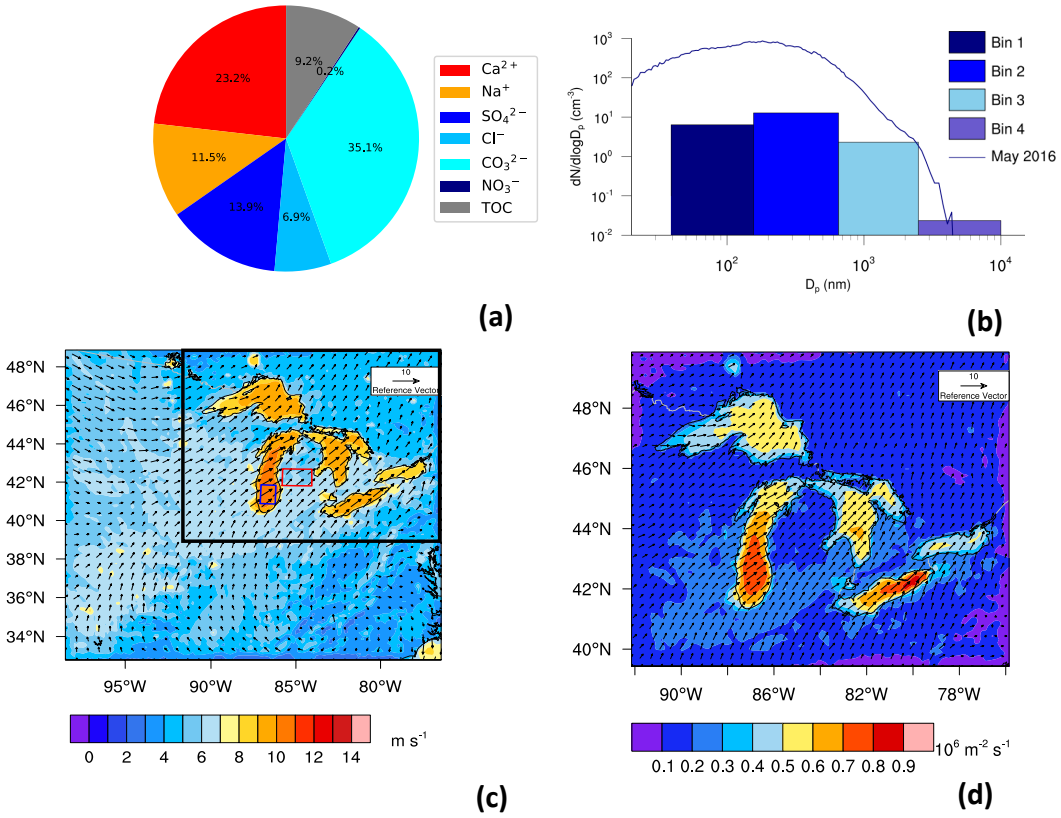

Figure 1. (a) Simulated mass fraction of the emitted LSA components, with the same composition in each of the four MOSAIC aerosol size bins. (b) Aerosol number size distribution for Lake Michigan freshwater from May et al. (2016) (solid line), with equivalent aerosol number concentration for the four MOSAIC bins for the area shown in blue box in (c) from a simulation with LSA emissions only. (c) Simulated 22−m wind speed (ms^{-1}) and direction, and (d) simulated wind−generated aerosol number flux ($10^6 m^{-2} s^{-1}$) over the lakes, with wind vector overlay. The values in (b-d) are averaged over November 2015 for the surface model layer. The blue and red rectangles in (c) indicate the area for which the aerosol composition was analyzed. The black rectangle in (c) shows the analysis domain focusing on the Great Lakes region.

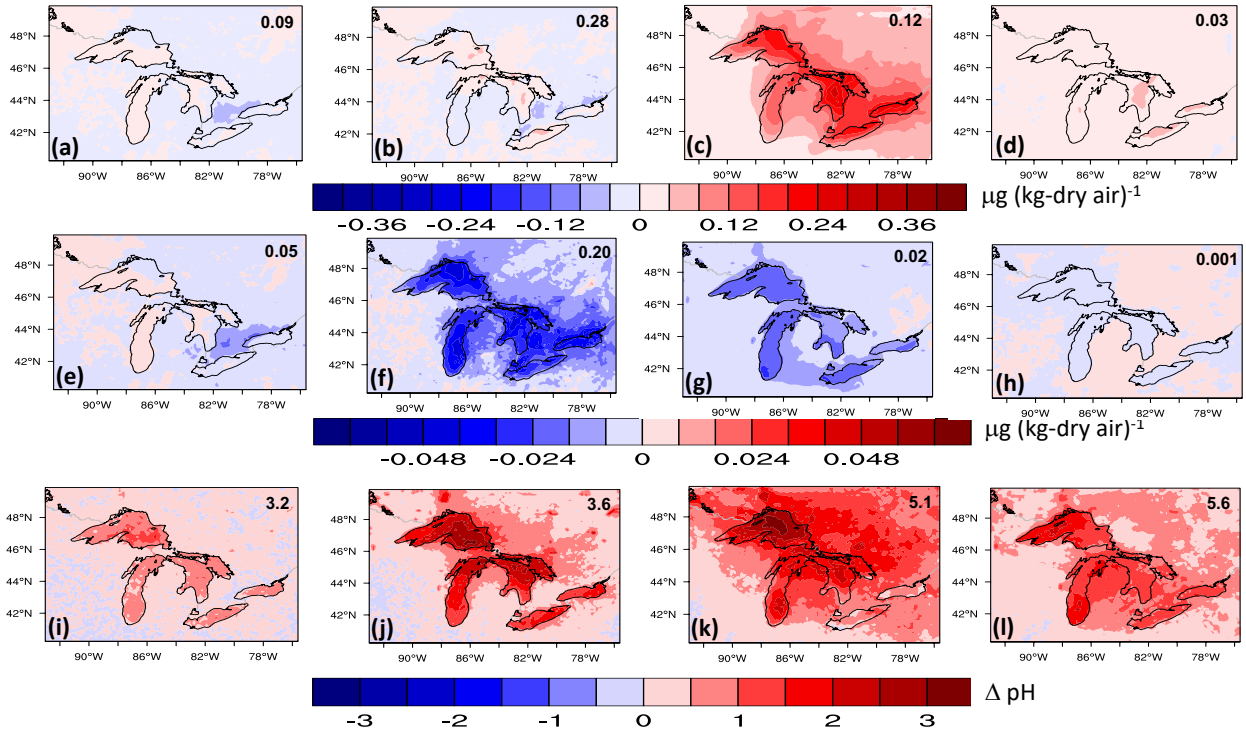

Figure 2. The difference between NEI+Lake and NEI simulations (NEI+Lake - NEI) of particulate NO_3^- (a–d), NH_4^+ (e–h) concentrations (μg (kg dry air)$^{-1}$), and pH (i–l) for the four MOSAIC bins (0.039–0.156 (Bin 1; a,e,i), 0.156–0.625 (Bin 2; b,f,j), 0.625–2.5 (Bin 3; c,g,k) and 2.5–10.0 (Bin 4; d,h,l) μm). Changes represent the difference in monthly average mixing ratios for the surface model layer in November 2015. The domain-average concentration for the NEI+Lake simulation is presented in the upper right hand corner for context.

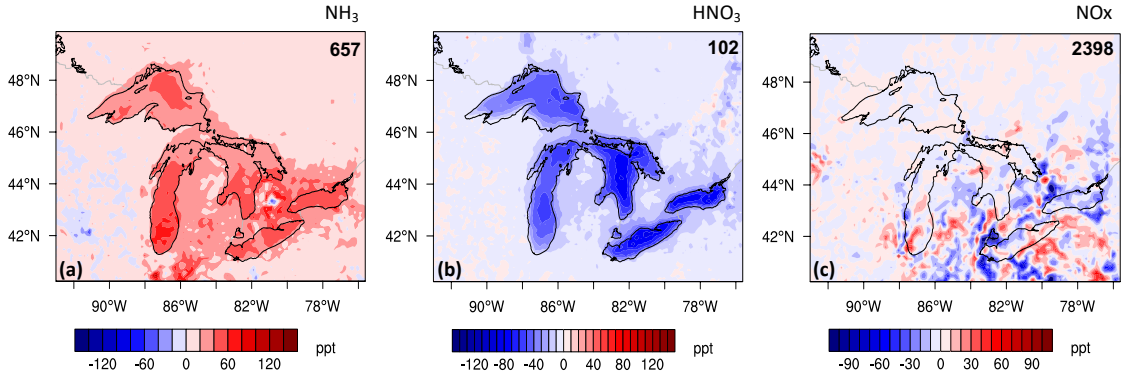

Figure 3. Same as in Fig. 2 but for (a) NH_3, (b) HNO_3, and (c) NOx.

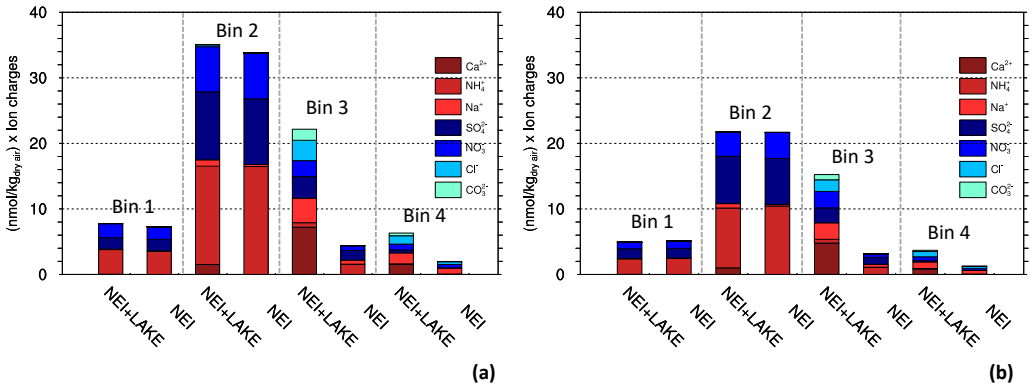

Figure 4. Simulated NEI+Lake and NEI average November 2015 surface model layer ion composition over the southern part of lake Michigan (a) and neighboring land (b), as the molar concentration of the aerosol particulate mass in dry air multiplied by ion charge is shown.

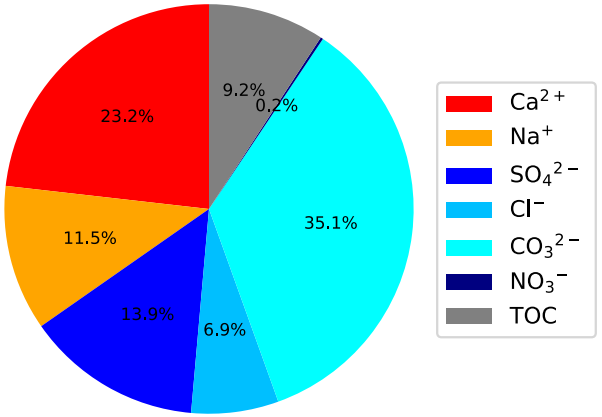
23.2%
9.2%
0.2%
35.1%
11.5%
13.9%
6.9%
Ca^{2+}
Na^{+}
SO_4^{2-}
Cl^{-}
CO_3^{2-}
NO_3^{-}
TOC

(a)

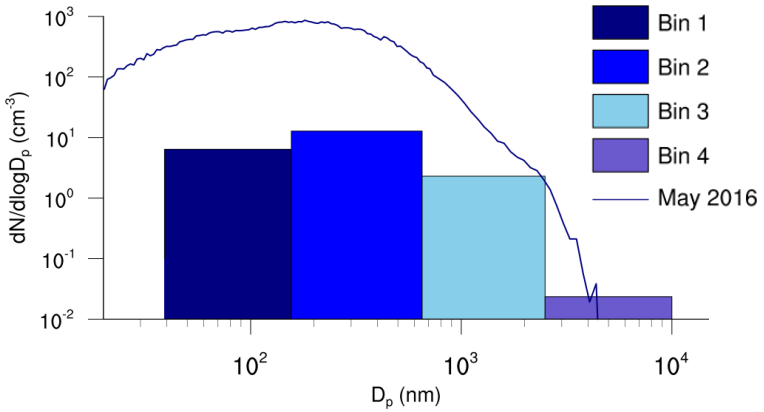
Bin 1
Bin 2
Bin 3
Bin 4
May 2016
$dN/dlogD_p$ (cm^{-3})
D_p (nm)

(b)

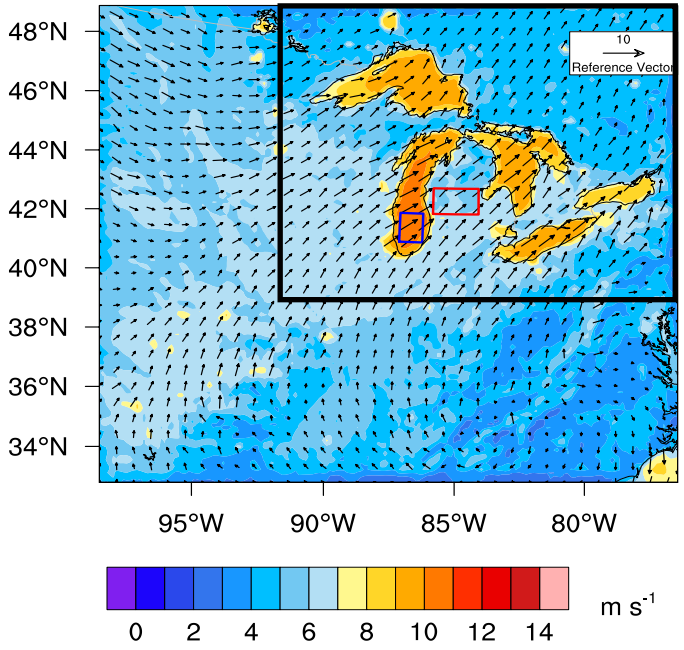
10
Reference Vector
48°N
46°N
44°N
42°N
40°N
38°N
36°N
34°N
95°W
90°W
85°W
80°W
0 2 4 6 8 10 12 14
m s^{-1}

(c)

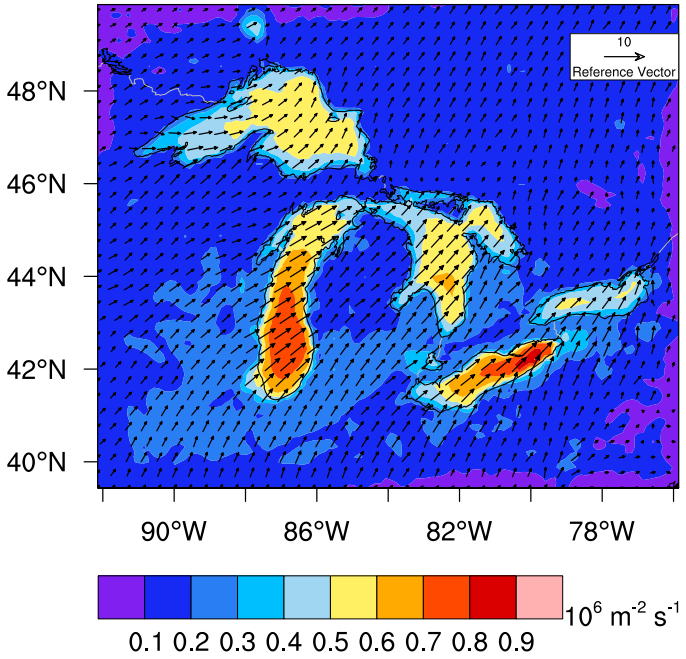
10
Reference Vector
48°N
46°N
44°N
42°N
40°N
90°W
86°W
82°W
78°W
0.1 0.2 0.3 0.4 0.5 0.6 0.7 0.8 0.9
10^6 m^{-2} s^{-1}

(d)

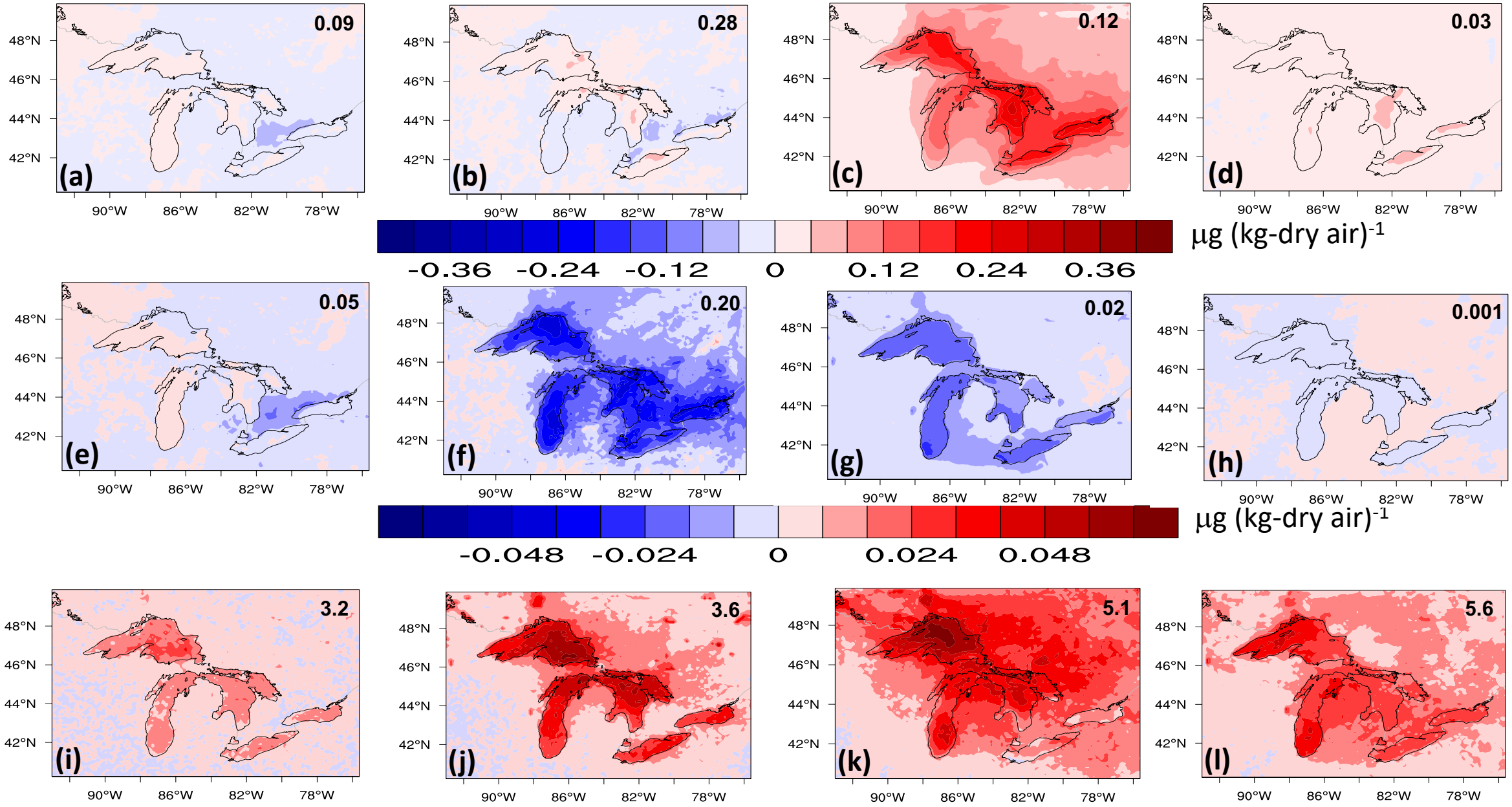
0.09
0.28
0.12
0.03
(a)
(b)
(c)
(d)
48°N
46°N
44°N
42°N
90°W
86°W
82°W
78°W
-0.36 -0.24 -0.12 0 0.12 0.24 0.36
µg (kg-dry air)-1
0.05
0.20
0.02
0.001
(e)
(f)
(g)
(h)
-0.048 -0.024 0 0.024 0.048
µg (kg-dry air)-1
3.2
3.6
5.1
5.6
(i)
(j)
(k)
(l)
-3 -2 -1 0 1 2 3
Δ pH

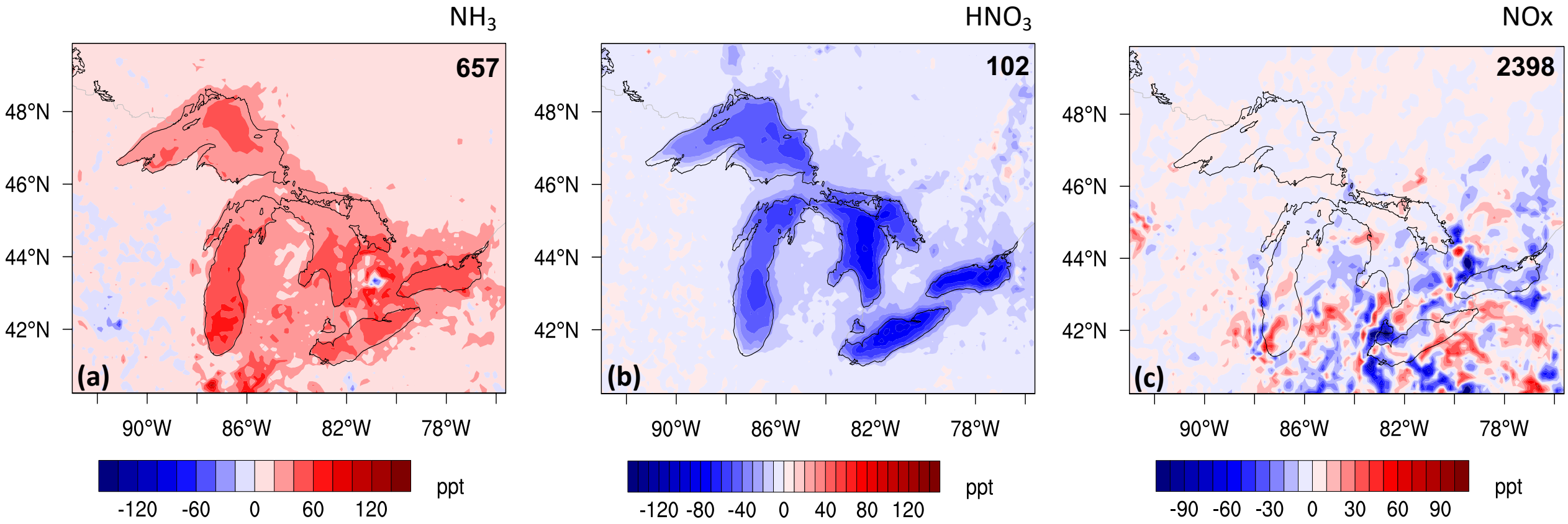
NH3
657
(a)
48°N
46°N
44°N
42°N
90°W
86°W
82°W
78°W
-120 -60 0 60 120
ppt
HNO3
102
(b)
48°N
46°N
44°N
42°N
90°W
86°W
82°W
78°W
-120 -80 -40 0 40 80 120
ppt
NOx
2398
(c)
48°N
46°N
44°N
42°N
90°W
86°W
82°W
78°W
-90 -60 -30 0 30 60 90
ppt

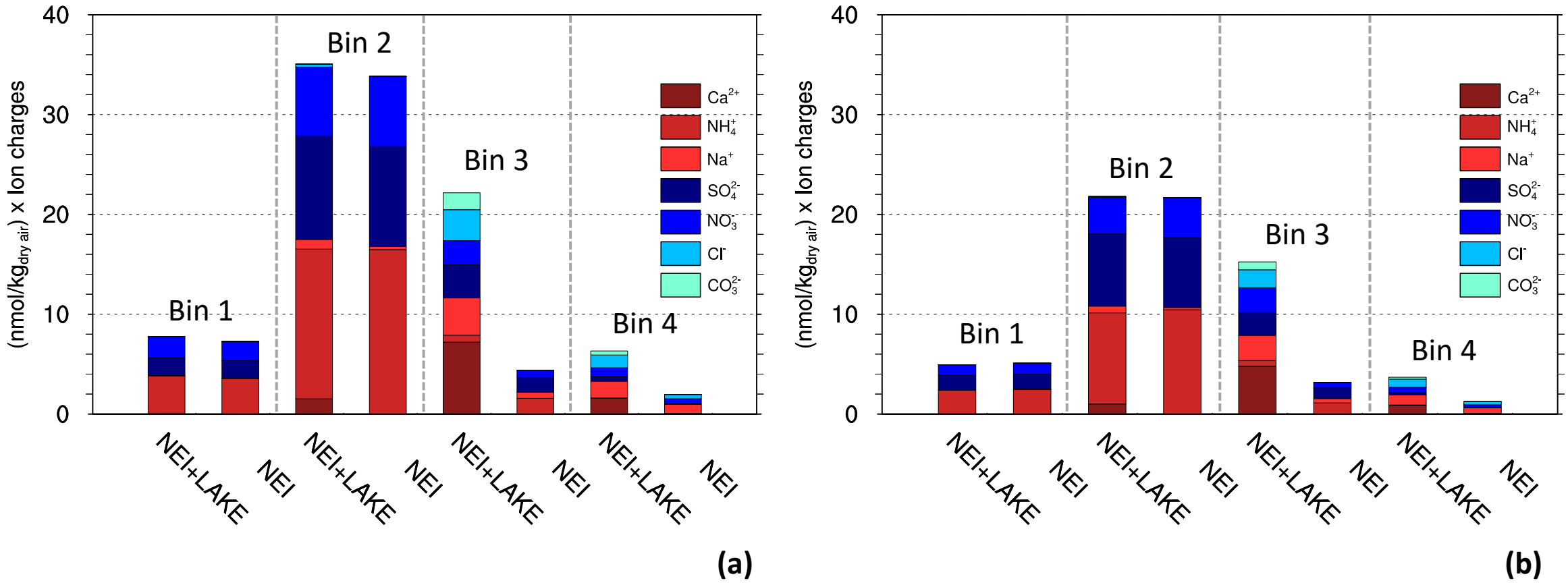
40
30
20
10
0
(nmol/kg$_{dry\ air}$) x Ion charges
Bin 1
Bin 2
Bin 3
Bin 4
Ca^{2+}
NH_4^+
Na^+
SO_4^{2-}
NO_3^-
Cl^-
CO_3^{2-}
NEI+LAKE
NEI
NEI+LAKE
NEI
NEI+LAKE
NEI
NEI+LAKE
NEI
(a)
(b)